Article

Non-Volatile Regulation of Magnetism via Electric Fields in Polycrystal FeSi/(011) PMN-0.32PT Heterostructures

Xiaobin Guo [1],*, Fengchao Su [1], Xiaoling Lu [1], Xingui Tang [1] , Zhenhua Tang [1], Wenhua Li [1], Yanping Jiang [1], Qiuxiang Liu [1], Yalu Zuo [2] and Li Xi [2],*

[1] School of Physics & Optoelectric Engineering, Guangdong University of Technology,
     Guangzhou Higher Education Mega Centre, Guangzhou 510006, China;
     2112015096@mail2.gdut.edu.cn (F.S.); 2112015092@mail2.gdut.edu.cn (X.L.); xgtang@gdut.edu.cn (X.T.);
     tangzh@gdut.edu.cn (Z.T.); liwenhuat@163.com (W.L.); ypjiang@gdut.edu.cn (Y.J.); liuqx@gdut.edu.cn (Q.L.)
[2] Key Laboratory for Magnetism and Magnetic Materials of Ministry of Education,
     School of Physical Science and Technology, Lanzhou University, Lanzhou 730000, China; zuoyl@lzu.edu.cn
* Correspondence: guoxb@gdut.edu.cn (X.G.); xili@lzu.edu.cn (L.X.)

check for updates

Abstract: The choice and configuration of the ferroelectric (FE) substrate and the ferromagnetic (FM) layer in FM/FE heterostructures play an important role in magnetism modification with regard to amplitude and efficiency. In this study, we fabricated FeSi films on low crystalline (011) $[Pb(Mg_{1/3}Nb_{2/3})O_3]0.7$-$[PbTiO_3]0.3$ (PMN-0.32PT) using radio frequency magnetron sputtering. In the annealed FeSi/(011) PMN-0.32PT heterostructures, the FeSi film presented with a (011) preferred orientated polycrystalline structure and low magnetocrystalline anisotropy. Both loop-like and butterfly-like magnetism modifications were observed by applying bipolar electric fields, and the weak and abnormal electrically mediated magnetism behaviors were significantly different from the prominent magnetic anisotropy transition in FeSi/(011) PMN-0.3PT. The comparative analyses suggest that the resulting high-quality single-crystalline PMN-xPT and FM films with low coercivity are of great significance for exploring giant, reversible, and non-volatile magnetism regulation.

Keywords: electric fields; polycrystal FeSi/(011) PMN-0.32PT; non-volatile; weak and unusual magnetism regulation

1. Introduction

Multiferroic materials with strong magnetoelectric (ME) couplings have attracted ever-increasing interest due to their potential application in ultra-sensitive sensors, microwave performance, and magnetic memory with ultralow energy consumption [1–4]. Most research activities have been focused on the converse ME coupling effect, i.e., electric field control of magnetism, with the aim of realizing giant, stable, reversible, and non-volatile magnetism regulation under the stimulation of electric fields [5–8]. The magnetism modification mechanism primarily includes interface charge accumulation/dissipation, exchange coupling, strain effect, orbital reconstruction, and electrochemical effect. Among them, the strain-mediated effect is widely recognized in artificial ferromagnetic/ferroelectric (FM/FE) multiferroic heterostructures with a thick FM layer [4]. For amorphous FM/FE heterostructures, the strain effect typically induces a uniaxial magnetoelastic energy in FM films, and the magnetic variation generally tracks the strain vs. electric-field (*S–E*) curves of the FE substrate [9–12]. For epitaxial FM/FE heterostructures, the magnetism is determined by the competition between strain-induced magnetoelastic energy and magnetocrystalline anisotropy energy [6,13–16]. To date, single crystal $[Pb(Mg_{1/3}Nb_{2/3})O_3]x$-$[PbTiO_3]1$-$x$ (PMN-xPT) has been the

most promising FE substrate candidate, owing to its excellent piezoelectric properties. The strain response is closely correlated with its FE polarization reversals, which depend on the crystal orientation as well as PT content [17–20]. In most cases, for (011)-oriented PMN-xPT, there is a strong loop-like *S–E* curve along the [01-1] direction under unipolar electric fields (asymmetric mediated between saturated and reversed coercive electric fields), which stems from the non-180° ferroelectric polarization switching between the out-of-plane and in-plane direction [8,21–24]. For (001)-oriented PMN-PT, it exists a loop-like *S–E* curve along the [−110]/[110] direction under bipolar electric fields (symmetric mediated between positive and negative saturation electric fields), which originates from the 109° ferroelectric polarization switching [5,6,12,20].

In addition, other *S–E* behaviors and unusual electrically modified magnetism behaviors have been reported in FM/PMN-xPT with different nominal composition. For instance, Yang et al. reported the non-volatile and volatile strain changes in two (001) [Pb($Mg_{1/3}Nb_{2/3}$)O_3]0.7-[$PbTiO_3$]0.3 (PMN-0.28PT) with the same nominal composition; the comparison of the *S–E* curves and the FE domain switching revealed that an absence of 109° ferroelectric domain switching was responsible for the volatile strain response [12]. Zhang et al. further demonstrated the coexistence of volatile and non-volatile converse ME effects in Fe/(001) PMN-0.3PT, which can reasonably explain the previous volatile magnetization–electric (*M–E*) curve in FM/PMN-xPT [18]. Compared with pure Fe films, the magnetocrystalline anisotropy field can be decreased by the addition of the non-magnetic element Si, it is easier to achieve the magnetization switching by electric field-induced piezoelectric strain. In $Fe_{80}Si_{20}$/(011) PMN-0.3PT, we reported a reversible and non-volatile magnetic transition between four-fold and two-fold anisotropy by applying unipolar electric fields [15,25]. On the basis of these results, it was fascinating to further study the influence of PMN-xPT substrate selection on FeSi magnetic properties as well as its magnetism regulation results.

In this work, we prepared FeSi/(011) PMN-0.32PT heterostructures with relatively low crystallinity. The initial magnetic properties and electrically modified magnetism behaviors for the FeSi/(011) PMN-0.32PT were significantly different from those of the previously reported FeSi/(011) PMN-0.3PT. Both loop-like and butterfly-like magnetism modifications under bipolar electric fields were observed at room temperature. By comparative analysis, we illustrate the correlation of the selected PMN-xPT, FeSi film crystallinity and magnetism modification behaviors.

2. Experimental

A (011)-oriented PMN-0.32PT (nominal composition) substrate was selected as the FE substrate, and a 65 nm-thick layer of $Fe_{80}Si_{20}$ (FeSi) was deposited onto the 0.5 nm thickness (011) PMN-0.32PT by radio frequency magnetron sputtering with a substrate temperature of 600 °C. After 300 °C annealing treatment, the crystallinity, initial magnetic properties, and electrically controlled magnetism were measured. As shown in Figure 1, the electric fields were applied along the [011] direction, where Ta and Pt layers served as the top and bottom electrodes. φ and θ are the in-plane azimuthal angles of the external magnetic field (*H*) and the equilibrium magnetization (*M*) with respect to the PMN-0.32PT [100] direction; the detailed preparation conditions and schematic configuration are similar to those described in Ref. [15]. The crystallographic structure of FeSi/(011) PMN-0.32PT was characterized using X-ray diffraction (XRD, PANalytical X′ Pert pro, Cu Kα radiation with wavelength λ = 0.15406 nm) and high-resolution transmission electron microscopy (HRTEM, FEI Tecnai G2 F30). The sample for TEM analysis was prepared by utilizing the focused ion beam etching technology mounted in a TESCAN MIRA 3 XMU field emission scanning electron microscope. The static magnetic hysteresis (*M–H*) loops were measured using a vibrating sample magnetometer (VSM, MicroSense EV-9) and a magneto-optical Kerr magnetometer (Durham Nano-MOKE TM2).
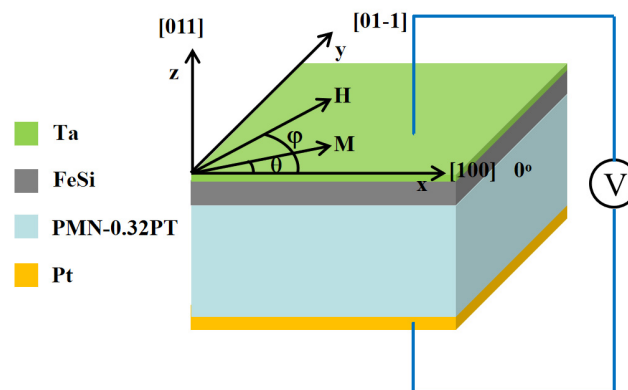
Figure 1. The coordinate system and schematic diagram of FeSi/(011) PMN-0.32PT heterostructures for the electric field control magnetization measurements.

3. Results and Discussion

3.1. Structural Analysis

Figure 2a shows the XRD patterns of FeSi/(011) PMN-0.32PT. In the normal θ-2θ XRD patterns, only the strong diffraction peaks indexed to PMN-0.32PT (011) and (022) were observed. It is clear that the diffraction peak width is larger and the peak intensity is lower than that of PMN-0.3PT reproduced in Ref. [15], suggesting that although the PMN-0.32PT substrate in this work is (011)-orientation, its crystallinity is significantly lower than the normal single crystal substrate. In order to avoid the influence of strong diffraction peaks originated from the PMN-0.32PT substrate, we conduct a glancing angle XRD measurement at a glancing angle of $\omega = 1°$. As shown in Figure 2a, the diffraction peak that appears at $2\theta = 44.65°$ is observed, which corresponds to the (011) diffraction peak of bcc-FeSi. The grain size along the normal direction of the (011) crystal face is approximately 12.3 nm based on the Debye–Scherrel fromula [26]. Since both the single crystal FeSi films grown in the [011] direction and polycrystal FeSi films with (011) texture structure will present the only one (011) diffraction peak, we cannot judge the crystallinity only from the single diffraction peak in the glancing angle XRD pattern. Apparently, the formation of full ordered epitaxial FeSi films is ruled out due to the broadened peak width as well as the later mentioned magnetic properties. We further conduct the transmission electron microscopy (TEM) and selected area electron diffraction (SAED) measurements to confirm the crystal structure. As seen in the low-magnification TEM cross-section images shown in Figure 2b,c, the FeSi film is composed of regularly distributed nano grains stacked layer by layer, with an average grain size of approximately 10 nm, which is close to the value calculated by the Debye–Scherrel fromula. The discontinued diffraction rings with spots reveal that the FeSi film is a polystalline structure with texture characteristics. It should be noted that the weak and regular arrayed diffraction spots were introduced by the adjacent PMN-0.32PT. From the high-resolution TEM image of the FeSi film in Figure 2d, one can see the obvious crystalline FeSi grains as well as distinct grain boundaries. The typical SAED pattern in the inset indicates a single-crystalline diffraction pattern with (011) preferred orientation. Thus, we conclude that the FeSi film is a polystalline structure composed of nano crystalline grains and there is a strong (011) crystallographic texture within the thickness range.

3.2. Electrically Modulated Magnetization

Figure 3a,b shows the angular dependence of the remanent magnetization (ARM) curve and *M–H* loops along the easy and hard axis directions. Compared with FeSi/PMN-0.3PT [15], the four-fold ARM curve still remained in our sample. The *M–H* loops vary greatly, the coercivity along the easy axis sharply increases from ≈5 to ≈24 Oe, and the magnetocrystalline anisotropy field extracted from the hard axis significantly decreased from ≈200 to ≈40 Oe. For an ideal polystalline magnetic film, it consists of a large number of small single crystals. When these small single crystals are

randomly distributed and are bound by highly defective boundaries, it results in normal continuous diffraction rings in an SAED pattern. In this case, the magnetic film is magnetic isotropy. Based on the aforementioned structure analysis, for the magnetic anisotropy of as-deposited FeSi films, it originates from the presence of an (011)-oriented texture in the polycrystalline FeSi films. We first focused on the electrically modulated magnetization in the $\varphi = 0°$ and $90°$ directions, i.e., the in-plane [100] and [01-1] crystallographic directions of (011) PMN-0.32PT. After several cycles of electric field stimulation, the ARM curves and *M–H* loops under the pulsed electric field remain nearly unchanged. In order to detect the weak magnetization varization under electric fields pulse, we measured the remanent magnetization upon the application of cyclic ±6 kV/cm electric field. In this process, the influence of the external magnetic field-induced Zeeman energy is ruled out, and M_r is determined by the contribution of crystalline anisotropy energy and strain-induced uniaxial magnetic anisotropy energy. As shown in Figure 3c,d, when ±6 kV/cm cyclic pulsed electric fields are applied to the heterostructures, at $\varphi = 0°$, M_r changed periodically between about 800 and 760 emu/cc. At $\varphi = 90°$, M_r varied periodically between approximately 960 and 1000 emu/cc. The change of M_r under the action of the +6 kV/cm is exactly opposite to that under the action of the −6 kV/cm. Hence, a reversible and non-volatile regulation of magnetization under symmetric bipolar electric fields is obtained.
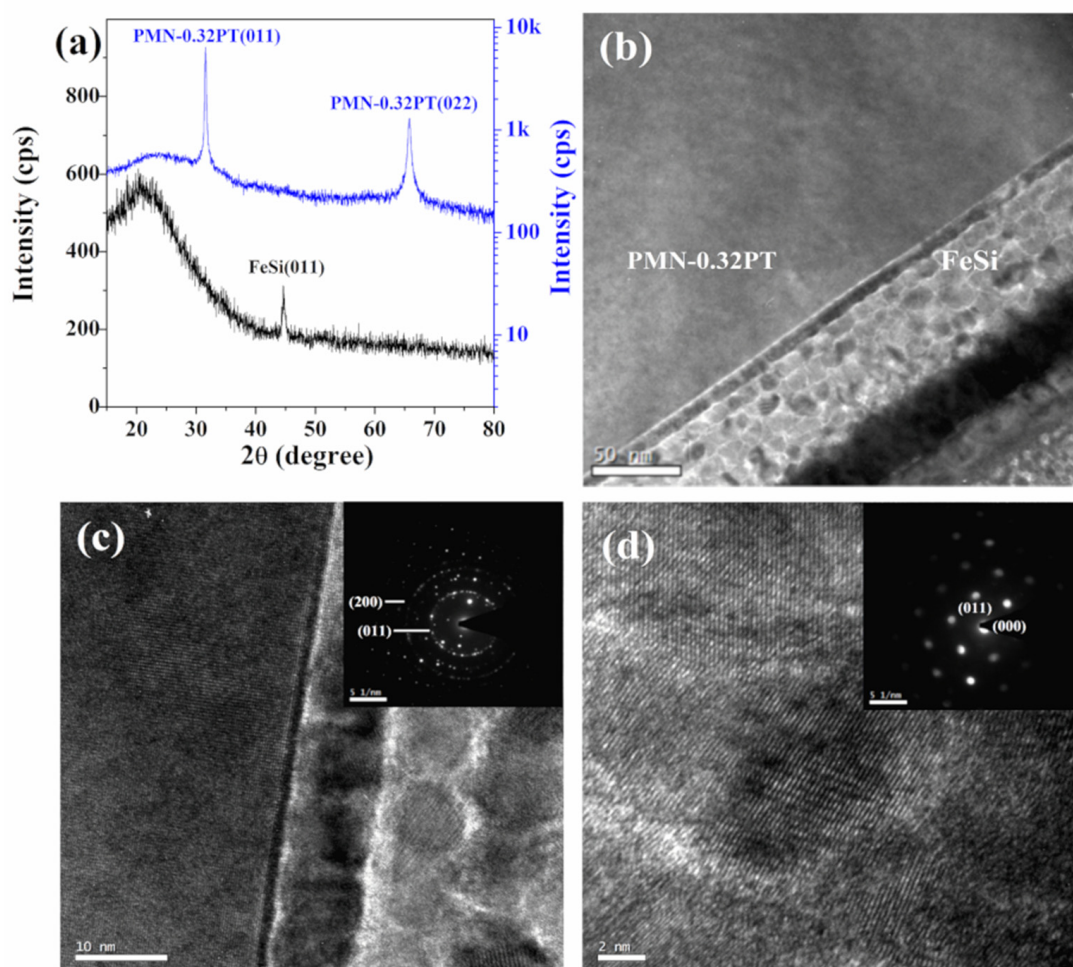

Figure 2. (a) X-ray diffraction (XRD) patterns of FeSi/(011) PMN-0.32PT and FeSi/(011) PMN-0.3PT heterostructures. **(b,c)** Low-magnification TEM cross-section of FeSi/(011) PMN-0.32PT heterostructures. **(d)** High-resolution TEM image of the FeSi films. The insets in **(c,d)** show the corresponding selected area electron diffraction (SAED) patterns.
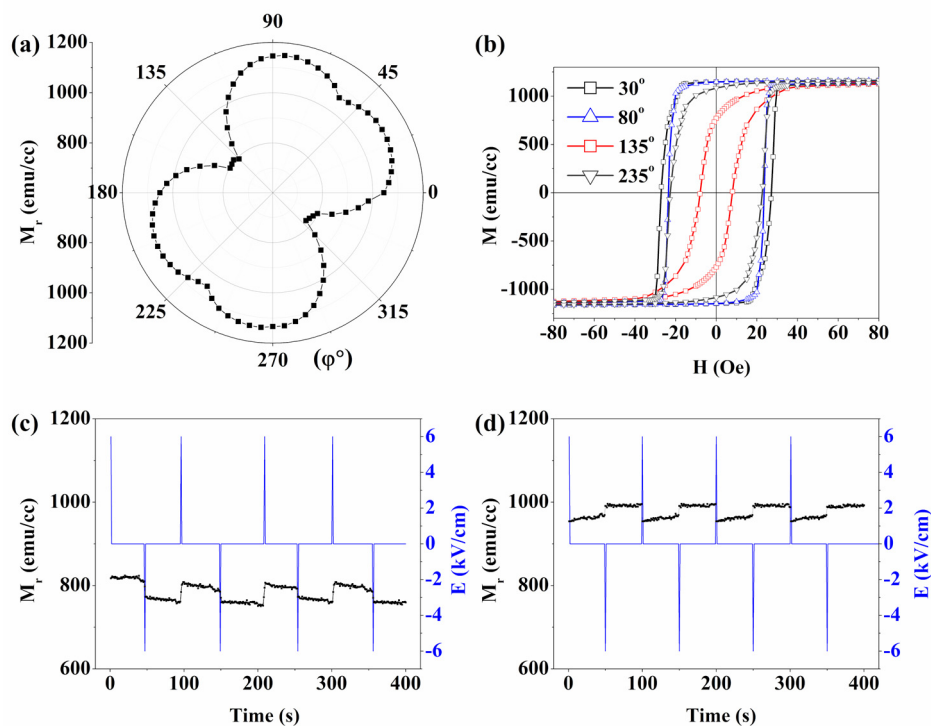
Figure 3. Angular dependence of the remanent magnetization (ARM) curve (**a**) and the magnetic hysteresis (*M–H*) loops (**b**) of FeSi/(011) PMN-0.32PT heterostructures. Non-volatile variation of M_r at $\varphi = 0°$ (**c**) and $\varphi = 90°$ (**d**) under electric fields pulses of ±6 kV/cm.

3.3. Electrically Modulated Shape of Kerr M–H Loops

For the FeSi/(011) PMN-0.32PT heterostructures, there was no expected [01-1]/[100] direction magnetization regulation between the saturated and reversed coercive electric fields. This can be ascribed to the following reasons. (i) There was no electric fields-controlled non-180° FE domain switching in the PMN-0.32PT substrate, resulting in no magnetization regulation by unipolar electric fields. (ii) The change of magnetization near the coercive electric field is either extremely small, or the accurate in-plane direction of the magnetism manipulation has not been found. Therefore, we measured the Kerr *M–H* loops relative to the electric fields through the longitudinal magneto-optical Kerr effect (MOKE), which is a more convenient and sensitive approach to detect weak magnetism changes with continuous electric fields [27,28]. For *H* along the $\varphi = 90°$, the electric field sweeping route is 8 kV/cm → 0 kV/cm → −8 kV/cm → 0 kV/cm → 8 kV/cm. The *M–H* loops always remain stable while electric fields gradually decrease from 8 to 0 kV/cm (Figure 4a). When further decreasing the electric fields to −8 kV/cm, the inclination of the *M–H* loop became smaller once the electric field was less than the coercive field of −2 kV/cm (Figure 4b). The *M–H* loops also remain unchanged with an electric field increase from −8 to 0 kV/cm (Figure 4c). After this, upon the application of the positive electric fields, the inclination of the *M–H* loop sharply returns to its original state once the electric fields exceeds 2 kV/cm (Figure 4d). This reveals that the *M–H* loops shape undergoes a loop-like modulation under symmetric bipolar electric fields. Figure 5a summarizes the variation of coercivity (H_c) and the remanence ratio (M_r/M_s) on the continuing electric fields. M_r/M_s shows no noticeable change, and H_c shows an obviously loop-like non-volatile behavior; i.e., the effect of positive and negative saturated electric fields on H_c are opposite, which is consistent with the tendency exhibited in Figure 3d.
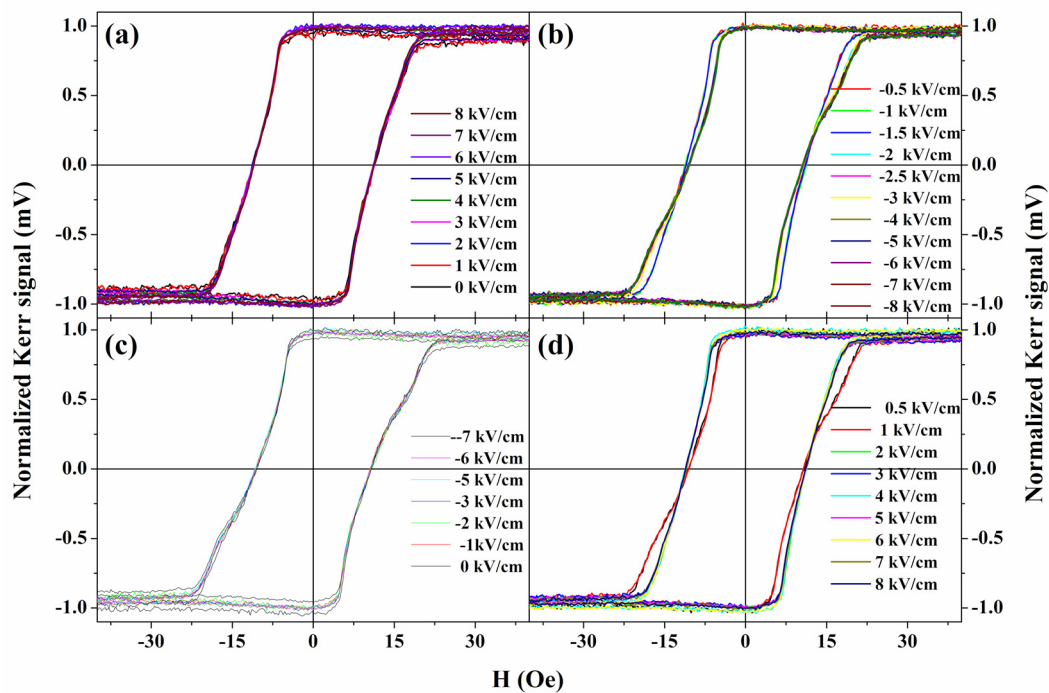
Figure 4. Longitudinal Kerr *M*–*H* loops as a function of bipolar electric fields ((**a**,**c**) correspond to the descent branches of electric fields. (**b**,**d**) correspond to the ascent branches of electric fields) with *H* along the φ = 90° direction.
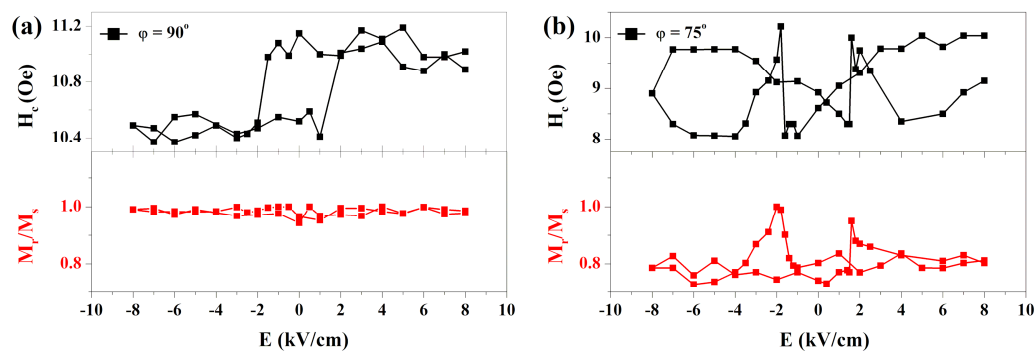

Figure 5. H_c and M_r/M_s versus the electric field curves along the φ = 90° (**a**) and φ = 75° (**b**) directions.

However, for the case of *M*–*H* loops along φ = 75°, the shape of the *M*–*H* loops remains unchanged for electric fields ranging from ±8 to 0 kV/cm, indicating that the effect of positive and negative saturation electric fields on magnetism is equal and the modification is non-volatile (Figure 6a,c). For near-coercive electric fields of ±2 kV/cm, the *M*–*H* loops change from inclined to rectangular with increasing H_c and M_r/M_s. Once the electric fields are switched off, the rectangular *M*–*H* loops can remain stable owing to the residual strain, leading to loop-like magnetism regulation between saturated and reversed electric fields [20]. As long as the electric fields exceed the opposite coercive electric fields and continue decreasing to −8 kV/cm or increasing to +8 kV/cm, the rectangular *M*–*H* loops will rapidly recover to their original inclined state, as is shown in Figure 6b,d. As a result, the shape of the *M*–*H* loops has a butterfly-like tendency under bipolar electric fields. The M_r/M_s and H_c relative to the electric fields are summarized in Figure 5b, while the variation curve of M_r/M_s on electric fields is consistent with the *S*–*E* curve of (011) PMN-0.32PT, indicating a reversible and non-volatile magnetism regulation under the action of unipolar electric fields. The butterfly-like curve is a consequence of the strain reponse of (011) PMN-0.32PT related to non-180° ferroelectric polarization switching [20–22]. When applying symmetric bipolar electric fields of ±8 kV/cm, one can observe the

butterfly-like anisotropy strain curves accompanied by two peaks around the around the coercive electric field of 2 kV/cm. It should be mentioned that due to the weak crystallinity of FeSi film, the H_c variation generally fits this tendency, but the ascent branch and descent branch are not consistent.
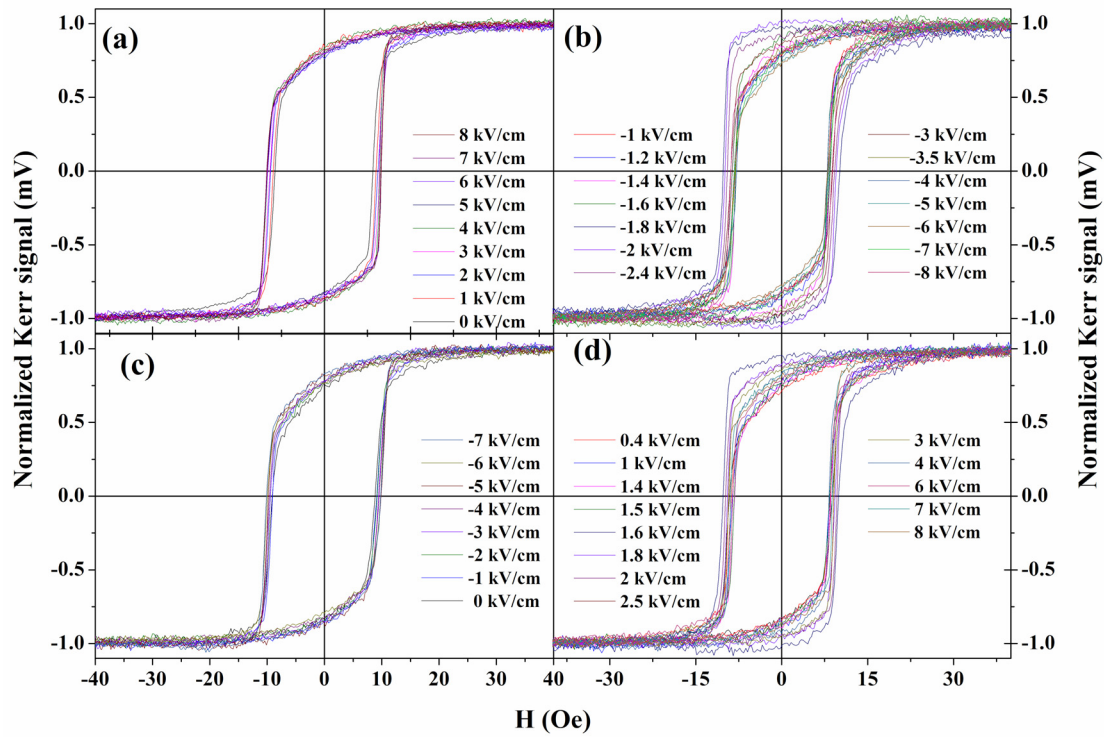

Figure 6. Longitudinal Kerr *M–H* loops as a function of bipolar electric fields ((**a**,**c**) correspond to the descent branches of electric fields. (**b**,**d**) correspond to the ascent branches of electric fields) with *H* along the φ = 75° direction.

3.4. Comparison and Analysis

In the FM/PMN-xPT heterostructure, the FM film microstructure, strain response of FE substrates, and strain transfer efficiency are the important factors to affect the converse ME coupling effect. Generally, only one kind of non-volatile *M–E* behavior was reported: either a loop-like *M–E* curve related to 109° ferroelectric polarization switching or a butterfly-like *M–E* curves related to non-180° ferroelectric polarization switching. For the case of FM/(001) PMN-xPT, Feng et al. reported the loop-like and butterfly-like *M–E* curves along the [100] and [−110] directions in CoFeB/(001) PMN-0.18PT, while the absence of the complementary *M–E* curve is ascribed to the cooperation of the FE phase transition induced by electric fields, internal electric fields in PMN-0.18PT, and the competition of different FE domains [29]. In FeSi/(011) PMN-0.32PT of this study, we observed both weak loop-like and weak butterfly magnetism regulation under a bipolar electric field, which is different from the huge butterfly magnetic anisotropy regulation under bipolar electric fields in FeSi/(011) PMN-0.3PT. For the FeSi/(011) PMN-0.32PT and the reported FeSi/(011) PMN-0.3PT, we compared and analyzed the results from the following two aspects: (i) crystallographic structure. For FeSi deposited on single crystal PMN-0.3PT, the crystalline grains only appear near the interface area, while the grain boundary gradually disappears and forms a large crystalline area with (011) oriented far away from the interface. For FeSi deposited on PMN-0.32PT with low crystallinity, as shown in Figure 2a, FeSi is a polycrystalline structure with (011) preferred orientation texture within the thickness range. The structural difference may be due to the defects, components, and impurities of the PMN-0.32PT substrate. (ii) initaial magnetic properties and magnetism modulation. FeSi/PMN-0.3PT presented a stable uniaxial magnetic anisotropy dominates. By applying asymmetrical unipolar electric

fields, a large, reversible and non-volatile magnetization switching along the [01-1] direction was realized, leading to the reversible and non-volatile magnetic transition between four-fold and two-fold anisotropy [15]. In contrast, for FeSi/(011) PMN-0.32PT with low crystallinity, the polycrystalline structure with obvious grain boundaries results in an increased coercivity and weak magnetism regulation amplitude. Instead of the expected magnetic anisotropy and magnetization transition, we observed a weak and loop-like non-volatile M–H loop shape variation at the $\varphi = 90°$ direction and butterfly-like M–H loop shape modification at the $\varphi = 75°$ direction by applying bipolar electric fields. By comparing the crystallographic structure and magnetism characteristics, we found that the larger the coercivity from grain boundaries and defects, the harder it is to obtain uniform electric-fields-controlled magnetism. The polycrystalline structure with texture and obvious grain boundaries in FeSi films results in a low strain transfer efficiency as well as a weak magnetism regulation amplitude. The coexistence of loop-like and butterfly-like magnetism regulation may be ascribed to the special ferroelectric domain reversal induced in-plane strain response in the low crystallinity of PMN-0.32PT, which needs further exploration in the future. The comparison results indicate that the selection of PMN-xPT substrate will directly influence the final magnetism under electric fields.

4. Conclusions

In summary, we fabricated FeSi/(011) PMN-0.32PT using radio frequency magnetron sputtering with a substrate temperature of 600 °C. After annealing at 300 °C treatment, it formed the (001)-oriented polycrystalline structure with regularly arranged crystalline grains. The FeSi films presented lower magnetocrystalline anisotropy and a weak magnetoelectric coupling effect. Combining VSM and MOKE measurements, both loop-like and the butterfly-like non-volatile magnetism modification under bipolar electric fields were observed. The weak and unusual electrically modulated magnetic behaviors were significantly different from the large and stable magnetic anisotropy transition in FeSi/(011) PMN-0.3PT heterostructures. The comparison analyses reveal that high-quality single-crystalline PMN-xPT and FM films with low coercivity are key to realizing the huge, reversible, and non-volatile magnetism modification via electric fields. This finding will be helpful for choosing a proper FE layer when designing advanced ME devices.

Author Contributions: Conceptualization, L.X.; data curation, X.G.; formal analysis, X.T. and Z.T.; funding acquisition, X.G., X.T., Z.T and L.X.; investigation, X.G.; resources, Y.Z.; supervision, X.T. and L.X.; writing—original draft, X.G., F.S. and X.L.; writing—review and editing, F.S., X.L., W.L., Y.J. and Q.L. All authors have read and agreed to the published version of the manuscript.

References

1.   Nan, T.; Hui, Y.; Rinaldi, M.; Sun, N.X. Self-biased 215 MHz magnetoelectric NEMS resonator for ultra-sensitive DC magnetic field detection. *Sci. Rep.* **2013**, *3*, 1985. [CrossRef]

2.   Liu, M.; Sun, N.X. Voltage control of magnetism in multiferroic heterostructures. *Philos. Trans. R. Soc. A* **2014**, *372*, 20120439. [CrossRef]

3.   Hu, J.M.; Chen, L.Q.; Nan, C.W. Multiferroic Heterostructures Integrating Ferroelectric and Magnetic Materials. *Adv. Mater.* **2016**, *28*, 15–39. [CrossRef] [PubMed]

4.   Song, C.; Cui, B.; Li, F.; Zhou, X.; Pan, F. Recent progress in voltage control of magnetism: Materials, mechanisms, and performance. *Prog. Mater. Sci.* **2017**, *87*, 33–82. [CrossRef]

5.   Zhang, S.; Zhao, Y.G.; Li, P.S.; Yang, J.J.; Rizwan, S.; Zhang, J.X.; Seidel, J.; Qu, T.L.; Yang, Y.J.; Luo, Z.L.; et al. Electric-field control of nonvolatile magnetization in $Co_{40}Fe_{40}B_{20}/Pb(Mg_{1/3}Nb_{2/3})_{0.7}Ti_{0.3}O_3$ structure at room temperature. *Phys. Rev. Lett.* **2012**, *108*, 137203. [CrossRef]

6. Guo, X.; Zuo, Y.; Li, D.; Cui, B.; Wu, K.; Yun, J.; Wang, T.; Xi, L. Electrical field control of non-volatile 90° magnetization switching in epitaxial FeSi films on (001) 0.7 [Pb (Mg$_{1/3}$Nb$_{2/3}$) O$_3$]-0.3 [PbTi$_{0.3}$O$_3$]. *Appl. Phys. Lett.* **2016**, *108*, 042403. [CrossRef]

7. Yang, S.W.; Peng, R.C.; Jiang, T.; Liu, Y.K.; Feng, L.; Wang, J.J.; Chen, L.Q.; Li, X.G.; Nan, C.W. Non-volatile 180 degrees magnetization reversal by an electric field in multiferroic heterostructures. *Adv. Mater.* **2014**, *26*, 7091–7095. [CrossRef]

8. Chen, A.; Wen, Y.; Fang, B.; Zhao, Y.; Zhang, Q.; Chang, Y.; Li, P.; Wu, H.; Huang, H.; Lu, Y.; et al. Giant nonvolatile manipulation of magnetoresistance in magnetic tunnel junctions by electric fields via magnetoelectric coupling. *Nat. Commun.* **2019**, *10*, 243. [CrossRef]

9. Thiele, C.; Dörr, K.; Bilani, O.; Rödel, J.; Schultz, L. Influence of strain on the magnetization and magnetoelectric effect inLa$_{0.7}$A$_{0.3}$MnO$_3$/PMN−PT(001)(A=Sr,Ca). *Phys. Rev. B* **2007**, *75*, 054408. [CrossRef]

10. Xi, L.; Guo, X.; Wang, Z.; Li, Y.; Yao, Y.; Zuo, Y.; Xue, D. Voltage-Driven In-Plane Magnetization Easy Axis Switching in FeNi/Piezoelectric Actuator Hybrid Structure. *Appl. Phys. Express* **2013**, *6*, 015804. [CrossRef]

11. Zhang, S.; Zhao, Y.; Xiao, X.; Wu, Y.; Rizwan, S.; Yang, L.; Li, P.; Wang, J.; Zhu, M.; Zhang, H.; et al. Giant electrical modulation of magnetization in Co40Fe40B20/Pb(Mg1/3Nb2/3)0.7Ti0.3O3(011) heterostructure. *Sci. Rep.* **2014**, *4*, 3727. [CrossRef]

12. Yang, L.; Zhao, Y.; Zhang, S.; Li, P.; Gao, Y.; Yang, Y.; Huang, H.; Miao, P.; Liu, Y.; Chen, A.; et al. Bipolar loop-like non-volatile strain in the (001)-oriented Pb(Mg1/3Nb2/3)O3-PbTiO3 single crystals. *Sci. Rep.* **2014**, *4*, 4591. [CrossRef]

13. Parkes, D.E.; Cavill, S.A.; Hindmarch, A.T.; Wadley, P.; Mcgee, F.; Staddon, C.R.; Edmonds, K.W.; Campion, R.P.; Gallagher, B.L.; Rushforth, A.W. Non-volatile voltage control of magnetization and magnetic domain walls in magnetostrictive epitaxial thin films. *Appl. Phys. Lett.* **2012**, *101*, 072402. [CrossRef]

14. Guo, X.; Li, D.; Xi, L. Magnetism manipulation in ferromagnetic/ferroelectric heterostructures by electric field induced strain. *Chin. Phys. B* **2018**, *27*, 097506. [CrossRef]

15. Guo, X.; Cui, B.; Guan, C.; Li, D.; Wu, K.; Yun, J.; Wang, T.; Peng, Y.; Zuo, Y.; Xi, L. Electric field modulation of reversible and non-volatile magnetic anisotropy transition in (011) 0.7[Pb(Mg1/3Nb2/3)O3]–0.3[PbTi0.3O3]/FeSi heterostructures. *J. Phys. D Appl. Phys.* **2017**, *50*, 335001. [CrossRef]

16. Zhang, B.; Meng, K.; Yang, M.; Edmonds, K.W.; Zhang, H.; Cai, K.; Sheng, Y.; Zhang, N.; Ji, Y.; Zhao, J. Piezo Voltage Controlled Planar Hall Effect Devices. *Sci. Rep.* **2016**, *6*, 28458. [CrossRef] [PubMed]

17. Li, Z.; Xu, Z.; Yao, X.; Cheng, Z.Y. Phase transition and phase stability in [110]-, [001]-, and [111]-oriented 0.68Pb(Mg$_{1/3}$Nb$_{2/3}$)O$_3$−0.32PbTiO$_3$ single crystal under electric field. *J. Appl. Phys.* **2008**, *104*, 024112. [CrossRef]

18. Zhang, S.; Chen, Q.; Liu, Y.; Chen, A.; Yang, L.; Li, P.; Ming, Z.S.; Yu, Y.; Sun, W.; Zhang, X.; et al. Strain-Mediated Coexistence of Volatile and Nonvolatile Converse Magnetoelectric Effects in Fe/Pb(Mg$_{1/3}$Nb$_{2/3}$)0.7Ti$_{0.3}$O$_3$ Heterostructure. *ACS Appl. Mater. Interfaces* **2017**, *9*, 20637–20647. [CrossRef]

19. Liu, Y.; Zhao, Y.; Li, P.; Zhang, S.; Li, D.; Wu, H.; Chen, A.; Xu, Y.; Han, X.F.; Li, S.; et al. Electric-Field Control of Magnetism in Co$_{40}$Fe$_{40}$B$_{20}$/(1-x)Pb(Mg$_{1/3}$Nb$_{2/3}$)O$_3$-xPbTiO$_3$ Multiferroic Heterostructures with Different Ferroelectric Phases. *ACS Appl. Mater. Interfaces* **2016**, *8*, 3784–3791. [CrossRef]

20. Liu, M.; Nan, T.; Hu, J.-M.; Zhao, S.-S.; Zhou, Z.; Wang, C.-Y.; Jiang, Z.-D.; Ren, W.; Ye, Z.-G.; Chen, L.-Q.; et al. Electrically controlled non-volatile switching of magnetism in multiferroic heterostructures via engineered ferroelastic domain states. *NPG Asia Mater.* **2016**, *8*, e316. [CrossRef]

21. Wu, T.; Bur, A.; Zhao, P.; Mohanchandra, K.P.; Wong, K.; Wang, K.L.; Lynch, C.S.; Carman, G.P. Giant electric-field-induced reversible and permanent magnetization reorientation on magnetoelectric Ni/(011) [Pb(Mg$_{1/3}$Nb$_{2/3}$)O$_3$](1−x)–[PbTiO$_3$]x heterostructure. *Appl. Phys. Lett.* **2011**, *98*, 012504.

22. Liu, M.; Howe, B.M.; Grazulis, L.; Mahalingam, K.; Nan, T.; Sun, N.X.; Brown, G.J. Voltage-impulse-induced non-volatile ferroelastic switching of ferromagnetic resonance for reconfigurable magnetoelectric microwave devices. *Adv. Mater.* **2013**, *25*, 4886–4892. [CrossRef]

23. Liu, M.; Hoffman, J.; Wang, J.; Zhang, J.; Nelson-Cheeseman, B.; Bhattacharya, A. Non-volatile ferroelastic switching of the Verwey transition and resistivity of epitaxial Fe3O4/PMN-PT (011). *Sci. Rep.* **2013**, *3*, 1876. [CrossRef]

24. Zhou, W.; Xiong, Y.; Zhang, Z.; Wang, D.; Tan, W.; Cao, Q.; Qian, Z.; Du, Y. Multilevel Resistance Switching Memory in $La_{2/3}Ba_{1/3}MnO_3/0.7Pb(Mg_{1/3}Nb_{2/3})O_3$-$0.3PbTiO_3$ (011) Heterostructure by Combined Straintronics-Spintronics. *ACS Appl. Mater. Interfaces* **2016**, *8*, 5424–5431. [CrossRef]

25. Guo, X.; Tang, X.; Liu, Q.; Jiang, Y.; Zuo, Y.; Xi, L. The influence of interface strain on the magnetization switching process in FeSi/(011) PMN-0.3 PT heterostructures. *J. Phys. D Appl. Phys.* **2020**, *53*, 255003. [CrossRef]

26. Birkholz, M. *Thin Film Analysis by X-ray Scattering*; WILEY-VCH Verlag GmbH & Co. KGaA: Weinheim, Germany, 2006.

27. Gao, Y.; Hu, J.M.; Wu, L.; Nan, C.W. Dynamic in situ visualization of voltage-driven magnetic domain evolution in multiferroic heterostructures. *J. Phys. Condes. Matter* **2015**, *27*, 504005. [CrossRef]

28. Xu, H.; Feng, M.; Liu, M.; Sun, X.; Wang, L.; Jiang, L.; Zhao, X.; Nan, C.; Wang, A.; Li, H. Strain-Mediated Converse Magnetoelectric Coupling in $La0.7Sr_{0.3}MnO_3/Pb(Mg_{1/3}Nb_{2/3})O_3$–$PbTiO_3$ Multiferroic Heterostructures. *Cryst. Growth Des.* **2018**, *18*, 5934–5939. [CrossRef]

29. Feng, C.; Liu, Y.; Huang, H.; Zhu, Z.; Yang, Y.; Ba, Y.; Yan, S.; Cai, J.; Lu, Y.; Zhang, J.; et al. Unusual Behaviors of Electric-Field Control of Magnetism in Multiferroic Heterostructures via Multifactor Cooperation. *ACS Appl. Mater. Interfaces* **2019**, *11*, 25569–25577. [CrossRef]

Publisher's Note: MDPI stays neutral with regard to jurisdictional claims in published maps and institutional affiliations.